Tactile, Orientation, and Optical Sensor Fusion for Tactile Breast Image Mosaicking

Rory Hampson, Graeme West, and Gordon Dobie

***Abstract*— Breast cancer screening using Tactile Imaging (TI) is an advancing field of low-cost non-invasive medical imaging. Utilizing arrays of capacitive pressure transducers to perform a differential stress measurement of suspicious tissue, TI has been shown to be effective in measuring lesion size and stiffness, and subsequent differentiation of malignant and benign conditions, in repeated clinical studies. In order to further improve the lesion classification accuracy of clinical TI, this paper presents a novel method of mosaicking tactile images to form a large composite tactile map using the vein structure within the breast to spatially register tactile data. This paper demonstrates practical non-rigid tactile image mosaicking, using probe contact force and relative orientation sensor fusion to correct for the tissue deformation during tactile scanning, miniaturized and applied to a pre-clinical TI prototype. Testing of the proposed TI prototype on representative, tissue-mimicking, silicone breast phantoms, with varying baseline elasticity and internal vein structure, yields typical image registration accuracies of 0.33% ± 0.15%. In similar testing, the proposed system measures the background elasticity of the samples with worst case error < 4.5% over the range 9 kPa to 60 kPa, required for accurate lesion characterization. This work will lead into further clinical validation of TI for measurement and classification of in-situ phantom and breast lesions, utilizing the delivered metrics from this work to improve differentiation accuracy.**

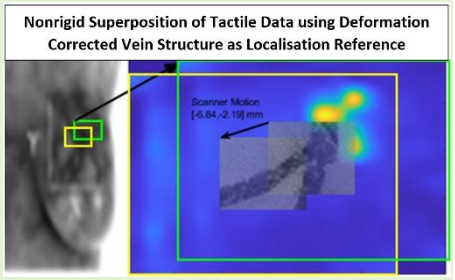

***Index Terms*— Breast Cancer, Force Measurement, Elastography, Medical Imaging, Structure from Motion.**

I. Introduction

TACTILE imaging (TI) is a continuously developing medical imaging technique used to perform soft tissue differentiation and force measurement in several medical fields [1]–[4] particularly in prostate and breast cancer diagnosis. In this context TI uses capacitive pressure sensors, or arrays of them, to measure differential contact stress which is used to identify and evaluate hardened tissues in the breast and prostate, a factor well linked to cancer diagnosis [5], [6]. Other interpretations of TI exist [7]–[9] each performing fundamentally the same task of differentiating tissues based on applied stress and forming a 'hardness image'. If a tactile image contains the boundaries of a suspicious tissue, meaning a suspected lesion is fully within a tactile image, then size, shape, and elasticity analysis can be performed on the lesion reasonably accurately within 10% and 20% respectively [10], important in cancer diagnosis and management [11]. This information about the lesion can be used to differentiate malignant and benign conditions [1], [12] which is estimated to reduce the benign biopsy rate by 23% with no missed cancers [1]. In current practice, TI is used as an optional screening tool to separate patients who may need further testing in a non-invasive and comfortable manner, and is generally more mature than other developing handheld tumor detection systems [13].

Despite TI being a comfortable and non-invasive tool for accurate screening, it is currently not used in place of x-ray mammography; the current gold standard in breast screening [14]. From a technical viewpoint this is due to a limitation in current TI, the inability to view the entire breast at once (a byproduct of the need for comfort, moving away from plate squeezing [15]) or generate a reliable composite image of the full breast. This is required for localization of the lesion on the breast and subsequent lesion tracking over time. Quadrant based tracking systems for TI have existed for some time, effectively a digital version of the breast cancer referral form [16]. In such systems, localization is manual and accuracy is dependent on proper operator procedures, not always followed in practice. It is imperative that TI be given the ability to spatially relate and localize lesions reliably on the breast if TI is to advance beyond its current capabilities and be used as an adjunct to mammography. Additionally, allowing the TI systems to see larger breast features by generating composite images will increase the flexibility of TI in general use. There are other issues limiting the widespread use of TI clinically, other than the technical issue addressed by this paper, including dominance of mammography in many healthcare systems [17], and small volumes of evidence compared with other modalities, that will also need to be addressed for TI to gain wider use.

A. Tactile Image and Feature Registration Techniques

Other than manual registration, and imaging the whole breast simultaneously, several methods exist for creating composite

This paper was submitted for review on 28/09/2022. This work was supported by PPS UK Ltd. and EPSRC under EP/Po11276/1.

Rory Hampson and Gordon Dobie are with Centre for Ultrasonic Engineering (CUE), Graeme West is with Advanced Nuclear Research Centre (ANRC), University of Strathclyde, G1 1XW , GB.

tactile images with none gaining traction in clinical breast TI.

Historically, external 3D tracking systems have been used to track the position of a TI scan probe as it passes over the breast. This method mosaicked tactile frames relative to the tracker base, rather than to the patient, meaning that the accuracy significantly degrades if the patient moved relative to the scan base during examination [18]. Additionally, 3D tracking systems are prohibitively expensive, reducing the cost effectiveness of TI in comparison to other static screening techniques [17], [19]. This method presented a useful method of averaging tactile frames that was used in future works.

A better method was later developed where correlation between sequential frames was used to determine the translation between frames [10]. The registered overlapping frames were then averaged to reduce noise. This method had the distinct advantage of only using the tactile sensor array itself, without needing external tracking systems, and was referenced to the patient meaning accuracy is maintained when the patient moves providing the sensor remains in contact. The correlation between frames was reliant on maintaining consistent scan pressures, as the tactile features visible in tactile images are stress dependent. This meant that tracking coherence was easily lost if the scan stress changed significantly, so this method was never used in clinical trials of breast TI [1], [12].

Examining other applications of TI, in prostate imaging, tactile frame registration is achieved using geometry and registration is with respect to relatively fixed structures such as the sphincter [3], [20]. Obviously, this is not appropriate for breast imaging as the breast is mobile and shape is not well constrained. However if a fixed structure on the breast can be identified and tracked, tactile images can be registered to that structure and be immune to external motion.

This idea has been investigated [21], using the vein network of the breast as a reference structure and an integrated infrared (IR) camera for tracking [22], which drew parallels with other works where IR was used for tumor monitoring during chemotherapy [23]. This method was effective in forming a coherent vein structure image, but was not suitable for mosaicking tactile images due to low tactile resolution. This system used non-rigid image mosaicking, that will be further developed in this work to form composite elasticity images.

B. Non-Rigid Vein Image Mosaicking

The key issue with using a structure such as the vein network for image registration is that the structure deforms during the tactile imaging process, skewing registration accuracy. The imaging part itself is trivial [22]. It is a key challenge in this area to produce an undeformed structure that can be referenced between scans, effectively removing the effect of the tactile imaging process on the breast vein structure. There have been several solutions proposed to this, not just in vein reconstruction but in wider deformable imaging, including: using finite element modelling (FEM) [24] to model deformation, shape from template (SFT) [25] to map images to a known template, structure from motion (SFM) [26] with high affine tolerance matching algorithms [27] or global optimization [28], and using elastic force based deformation approximation [21]. Detailed reviews discuss these [29], however the key takeaway is that authors are faced with a tradeoff between reconstruction accuracy and execution speed with simpler models being suitable for real-time operation [21], and more complex models that may offer better initial deformation reduction only being suitable for post processing activities. It is important to note that perfect deformation reduction is not necessarily required. The reduction only needs to be sufficient to drop the affine distortion to within the tolerance of a given image matching algorithm [30], that will estimate the relation between one frame and another. This often makes simple models more effective than originally expected.

II. Scope and Structure of the Paper

This work details the adaptation and integration of non-rigid image mosaicking techniques with tactile sensor arrays for the purpose of forming a composite tactile image using the vein network as a reference structure. New technology is introduced and validated for registration accuracy using simulated vein structures on silicone phantoms, with elasticity measurements of linear background materials being made simultaneously. It is known from previous works [10] that lesion elasticity can be estimated if the background elasticity is known, which this work will provide. Parametric analysis will be performed to determine TIS sensitivity to background material properties.

Section III details the proposed tactile imaging system (TIS). Sections IV and V detail the image registration algorithm and elasticity measurement technique respectively. Section VI demonstrates forming a composite elasticity image using the proposed TIS and methods. Sections VII and VIII detail the validation methodology and respective results. Final discussion on validity and study limitations is given in Section IX.

III. Hardware Implementation

A. TIS Construction

The proposed TIS is shown in Fig.1. It is based on previous designs [21], adapted so the scan face can accommodate a tactile array such as PPS PN4698 (Medical Tactile Inc. US-CA) used in SureTouch™ [10] or simpler arrays as shown in Fig. 1.

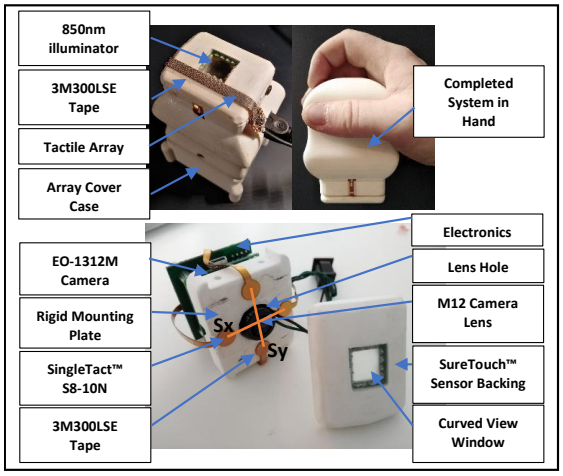

Fig. 1 – Proposed TIS Scanner Exploded View. The handheld system's scan face and internals are shown.

The TIS consists of a custom 850nm LED ring, embedded in a curved sensor array backing with an acrylic view port. This is used to illuminate the tissue/phantom to highlight the vein structure in the IR spectrum. The backing matches the dimensions of SureTouch™ (Sure Inc. US-CA) to accommodate a modified PN4698 12x16 element sensor array (40x50mm). Due to project limitations, the system was implemented using a PPS PN5420 1x12 array (6 are used) fixed to the backing using 3M 300LSE tape (3M Company, US-MN). This provides tactile information for detecting lesions. 4 SingleTact™ S8-10N pressure sensors (PPS UK ltd. UK) are sandwiched between the backing and a rigid plate using more tape. These are used to determine the total load applied to the phantom, and the TIS probe orientation relative to the surface. An Edmund Optics EO-1312M camera, with a known spectral response [31], is mounted to the plate with its lens projecting through to the viewport and is focused 5mm from the viewport surface. This is used to capture the deformation of, and TIS translation relative to, the vein network. Custom electronics featuring a BNO055 orientation sensor (Robert Bosch GmbH, DE) used to determine the orientation of the TIS relative to a fixed repeatable coordinate frame defined by the earths magnetic field and the gravity vector, and control circuitry for the LED ring complete the TIS.

B. TIS Electronics

The TIS internal electronics consists of the camera module, a custom sensor interface controller, an orientation sensor, and SingleTact interface electronics as shown in Fig.2. This also highlights the purpose of the major components. The camera module connects directly to a PC via USB and is controlled using uEye Cockpit software (IDS GmbH., DE), that records camera frames to an .avi file at 17.2FPS. An external tactile array controller is required to interface with the current implementation of tactile array. Tactile data from the PN5420 is recorded using PPS Chameleon software via a PPS D710 module at 100Hz. Data from SingleTact™ and orientation sensors are read via I^2C at 100Hz and 30Hz respectively and sent to a Serial terminal via USB. Power for the electronics and external components is 5V via USB.

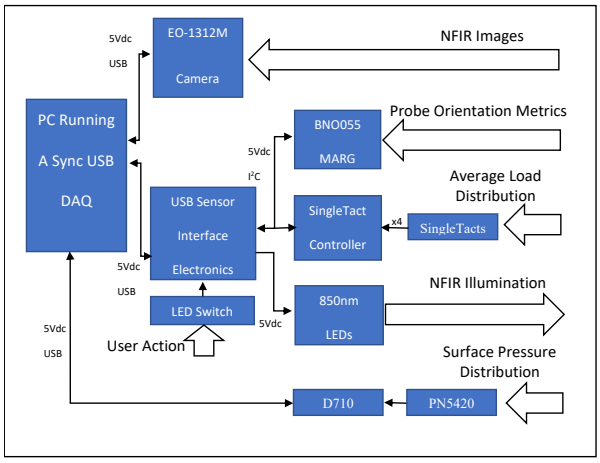

Fig. 2 - Proposed TIS Block Diagram. Diagram shows the high level components used and data flow associated with the TIS. Tactile array controllers are omitted, as these are optional.

C. Data Processing Framework

Data streams from the different components are captured using multiple pieces of software, and are combined and synchronized manually for use on a MATLAB script that runs the tactile mosaicking algorithm. This was a result of project limitations, presenting no academic challenge, and not affecting the end result. The system is run, and data processing performed, on a Windows 10 laptop with 8GB RAM. All sensor fusion occurs at the PC.

The data streams are saved with their own relative timestamps. Data synchronization is achieved manually using an 'impulse' event, where the tactile array is touched briefly near the camera view port. This is an event that is registered on the tactile array, camera, force sensors, and orientation sensor as an acceleration impulse. This is analogous to a 'clapper' [32]. The data streams are then interpolated and resampled to provide synchronized data homogenized to the IR image frame rate for fusion and processing.

IV. Tactile Image Registration Algorithm

The TI image registration consists of 3 key stages: Firstly the contact distortion on the vein images is reduced using estimation of contact mechanics, secondly the vein images are mosaicked together using a form of A-SIFT [21] yielding transforms between frames, and thirdly a rigid transform is applied to relate the tactile data to the vein images.

A. Deformation Reduction Using Contact Mechanics

Deformation of the vein images is performed using a contact mechanics approach similar to previous versions [21]. Using knowledge of the background material properties, the deformed image pixel location P' can be transformed to the undeformed location P using an estimation of the scan load distribution F as shown in equation 1. Here ν is the material Poisson ratio, E is the material Youngs Modulus (elasticity), and A is the local area where the scan force is being examined. The value of E is estimated in Section V, ν assumed to be 0.5.

$$P_{[x,y]} = \frac{P'_{[x,y]}}{1 - \nu\left(F_{[x,y]} \Big/ A_{Element} E\right)} \tag{1}$$

The force distribution F is a function of the scan face geometry, material properties, and insertion depth into the material surface, which is itself a distribution based on the geometry of the scan head and its orientation w.r.t. the surface. Equation 2 describes the force F at point (x,y) based on the average force from the SingleTact™ sensors, a calibration factor k (related to E) and variation in depth, dz, from the center.

The variation in depth, for a shape with uniaxial cylindrical curvature is given by equations 3 and 4, where r is radius of curvature (40mm) and x is the position in axis of curvature. This point cloud (surface) can then be rotated about its center by angles (θ, φ) respectively to obtain the variation in depth dz.

$$F_{[x,y]} = F_{Average} - kdz_{[x,y]} \tag{2}$$

$$z = -r + \sqrt{r^2 - x^2} \tag{3}$$

$$3D_{Position} = [x, y, z]^T, \quad |x| < \frac{r}{2}, \quad |y| < 25mm \quad (4)$$

The angles θ and φ are the angles in about x and y axes, with respect to the material surface, that are calculated based on the difference between coaxial force measurements from the SingleTacts (F_1, F_2; F_3, F_4), the calibration constant k, and the axial displacement between SingleTact pairs S as shown in equation 5. S_x = 28mm, S_y = 35mm, and are shown in Fig 1.

$$\theta = \sin^{-1}\left(\frac{F_2 - F_1}{2kS_y}\right), \quad \varphi = \sin^{-1}\left(\frac{F_4 - F_3}{2kS_x}\right) \quad (5)$$

By inverting equation 5, and using the onboard orientation sensor to provide a reference value for the angles zeroed with dF = 0, the value of k can be determined during an initial calibration process; important, as the orientation sensor yields absolute orientation, w.r.t. to a persistent coordinate frame defined by the earths magnetic field and the gravity vector, rather than relative to the material surface.

B. Vein Image Mosaicking

Once the deformation in the vein images has been reduced by the method in subsection A, the images can be passed to an image matching algorithm to estimate the spatial relationship (or transform) between frames. In this case SIFT is used to match image features, as this has been shown to be robust when affine deformation is small [30] and is well documented and understood in the literature. A detailed description of this process is presented elsewhere [21]. The image matching and registration algorithm produces a series of non-rigid transforms representing the relation between adjacent frames. This is done using RANSAC [33] to find the best fit homography matrix between matching image features identified using SIFT.

The 3x3 frame transform matrices T_i are multiplied with previous transforms to obtain the 'ith' transform as shown in equation 6. The N total transforms are then center adjusted to minimize edge distortion as shown in equation 7. This results in adjusted transform list T_{Adj} detailing frame relations.

$$T_{Equivalent\ (i)} = T_i * T_{i-1} \quad (6)$$

$$T_{Adj\ (i)} = T_{Equivalent\ (i)} * T^{-1}_{Equivalent\left(\frac{N}{2}\right)} \quad (7)$$

C. Tactile Image Mosaicking

Tactile images are resized to match the pixel size of the IR images, so they can be merged and retain proportionality. They are then mapped using a rigid transform relating tactile array and camera locations from (7), shown in equation 8. Overlapping tactile data points are averaged. An example is shown in Fig.3.

The angles from (5) are then added to the absolute measurements from the orientation sensor to determine the orientation of the material/breast surface in 3D space, which is used to cast the mosaicked images onto 3D structures rather than simple 2D planes.

$$T_{TI\ (i)} = T_{Adj\ (i)} * T_{TI-IR} \quad (8)$$

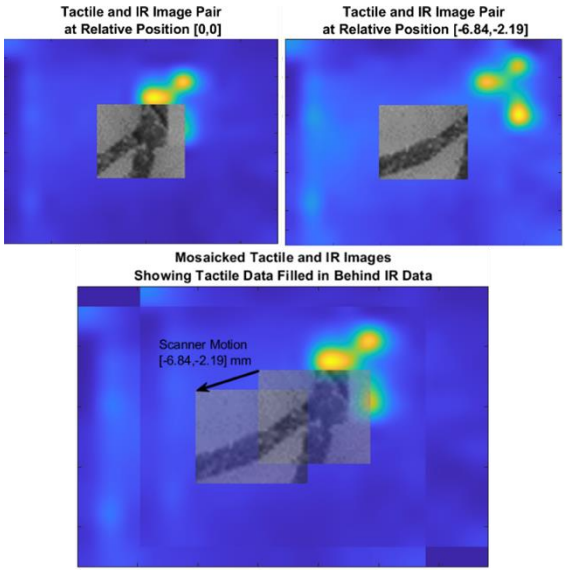

Fig. 3 - Tactile Image Vein Registration Example. The output of a PN4698 12x16 array showing phantom tactile features is mosaicked using translation from underlying vein images. Detail hidden in one image is filled in by the next as coincident data are merged..

V. Background Elasticity Measurement Algorithm

Estimation of breast background elasticity E is achieved by inverting equation 1 to obtain E based on the applied force and the subsequent observed deformation to the material as shown in equation 9. As the relative deformation is equivalent to the material lateral strain, characterized by the change in radial location of an image feature (identified using SIFT) dR_i ratioed with its original position R_i, and we have access to the applied stress ($F_{Total}/A_{Scanner}$), we can characterize the stress/strain relationship of the material. This is assumed to be linear for this work, but it need not be as a continuous stress/strain curve can be obtained. F_{Total} is the sum of the 4 force sensor measurements. Negativity is a result of the definition of dR_i and its sign convention, E is still positive.

$$E = -\nu \frac{F_{Total}}{A_{Scanner}\left(dR_i/R_i\right)} \quad (9)$$

This measurement is performed by pressing the proposed TIS into the material, normally such that angles θ, φ are near zero with minimal lateral translation. This is done at the start of a scan, and is updated locally whenever lateral displacement over 5 consecutive frames is near zero. This helps track and mitigate background elasticity variation across the breast.

VI. Integrated Elasticity Image

A. Calibration of the TIS

Prior to use the TIS must be calibrated (in addition to the tactile sensor array being recalibrated post assembly), as shown in Fig.4. The BNO055 orientation sensor is calibrated by placing the TIS in the orientations shown in sub-box 1-3 for 6 seconds. The SingleTact sensor array and tactile array are normalized by pressing the TIS normally into a silicone calibration pad up to a scan load of 1.5kg, measured with a

reference load cell beneath the pad. This must be done each time the TIS is power cycled.

Calibration of the value k is performed by rocking the TIS side to side in each axis over the range ±20° maintaining a relatively constant average scan load on the flat calibration pad.

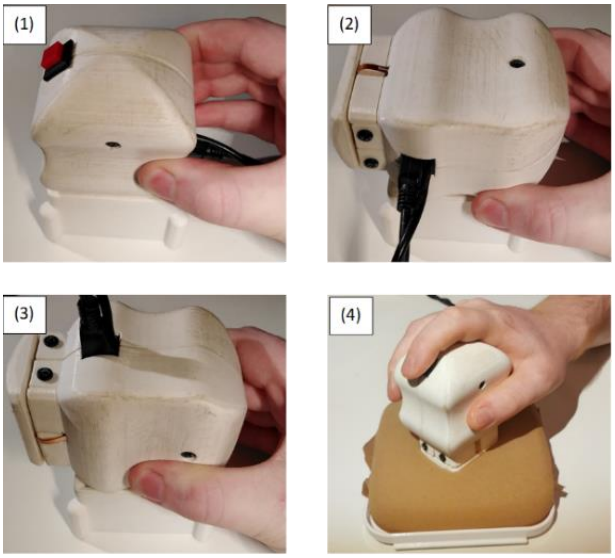

Fig. 4 - TIS Calibration Process. Steps 1-3 calibrate the orientation sensor by redefining orthogonal axes and the gravity vector. Step 4 normalizes the SingleTact and tactile array response.

In calibration steps 1-3, the BNO055 is going through its internal orientation calibration process, and so no data is collected. In this case, the sensor is locking on to the global coordinate frame. It is important that the TIS is held still, and its mounting is used to rest the TIS in orthogonal directions. Once the BNO055 signals that it has completed calibration, then step 4 can be performed.

Here, load data from the SingleTacts and tactile array, and orientation data is collected for two phases. Firstly, when the orientation is normal to the calibration block, loads from each SingleTact are normalized against a reference load cell (PPS D660) to account for non-linearities or shifts in the sensor performance. This is also the process for calibrating the tactile array. Then, once this is done, the TIS is rocked side to side on each axis, and orientation angles from the BNO055 are used to calibrate the value for 'K' using (5) by relating the angle to the axis force difference.

B. Forming the Elasticity Image

Following successful calibration of the TIS, a mosaicked tactile image can be formed. This is done by stroking the TIS over the surface of the material, or breast, maintaining a relatively consistent speed (to keep image overlap consistent) and scan pressure (to keep tactile data consistent). The device may rotate and tilt in use, as SIFT is rotation invariant and the affine algorithm in Section IV deals with the tilt.

Once the mosaic is formed, it can be turned from a tactile (pressure) image into an elasticity image using known methods [10] as shown in Fig.5 with the background elasticity set as E from section V. This shows that the vein mosaicking can be used for creating composite tactile images, as it would not be possible to mosaic 1D array data otherwise using existing methods [10].

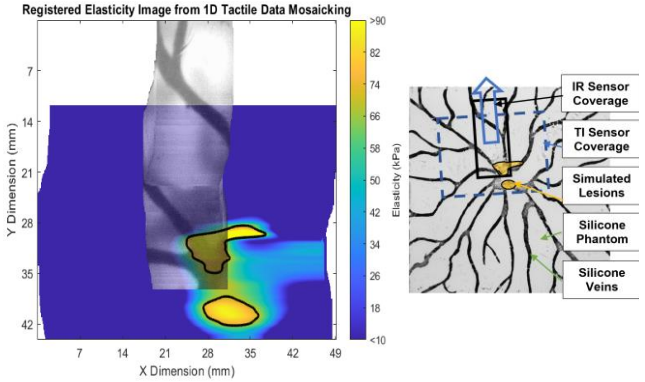

Fig. 5 - Composite Elasticity Image Formed by Proposed TIS (Left) Reference structure used for generation of composite elasticity image (Right). Uncalibrated inclusions were added to phantom materials based on Sample 1 described in Section VII-A.

Due to project scope limitations, phantoms with calibrated inclusions could not be made for this work, so detailed analysis of elasticity of inclusions from composite tactile images could not be fully validated, and so further array testing will not be covered in this work. However as the tactile image registration accuracy is independent of the tactile array, as it is based on the IR mosaic accuracy from (7) which does not use the tactile array, it is possible to investigate the image registration accuracy without the tactile array data or inclusions. Here we use the error in T_{Adj} from (7) as a suitable proxy for the tactile registration error, measured at the TIS origin at the centre of the scan face. The key objective has been achieved, with a method of forming composite tactile images presented here, the accuracy of which must now be tested.

VII. Test Methodology

A. Test Materials

Registration accuracy of the TIS is tested on flat linear phantom tissues made with embedded vein structures of varying feature densities as shown in Fig.6. These were made to approximately resemble the vein density observed in thermographic observations of breast tissue. The phantoms were made from Polydimethylsiloxane (PDMS) silicone (Smooth-On Inc., US-PA) with hardness, mixture ratios, additives, and dimensions as detailed in Table 1. PDMS is known to be suitable for making phantom breast tissue with elasticities in a normal breast tissue range [34].

These different phantoms allowed for parametric evaluation of registration and elasticity measurement accuracy vs. feature density and background elasticity, known to be variable in normal breast tissue. Additionally, it is known that the elasticity measurement accuracy of tactile imaging systems can be sensitive to base elasticity [10], [35], making this parametric analysis valuable by indicating generalized performance stats.

The vein network was made by mixing a small amount of carbon dust into the respective layer mix. The skin layer obscured the vein network partially using PMS488C light skin tone pigment (Smooth-On Inc. US-PA) to improve realism. Layers were mixed and cast sequentially, with layer C first, then the vein layer (cast separately and cut to shape) placed on top, then layer B_2 and A cast together to achieve the final

dimensions. The silicone mixtures were properly degassed before and after pouring into 130x130mm molds.

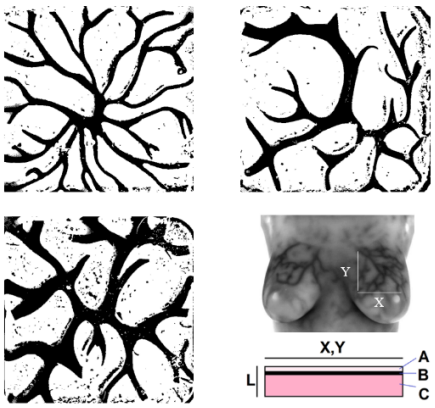

Fig. 6 - Phantom vein structures and reference material from thermographic vein images. Different vein distributions simulated with varying average vein feature density.

Table 1 - Phantom material composition and dimensions

MATERIAL COMPOSITIONS OF DEVELOPED PHANTOMS THICKNESSES: A = 4MM, B1 = 2MM, B2 = 2MM, C = 14MM				
Sample Number	**Sample Layer**	**Material A:B Ratio**	**Thinner By Mass**	**Additives By Mass**
1-3	A	000-35 1:1	+0%	PMS488C +1%
	B_1	00-10 1:3	+20%	Carbon Dust 1:100
	B_2	000-35 1:1	+0%	PMS488C +1%
	C	000-35 1:1	+10%	None
4-6	A	00-10 1:1	+0%	PMS488C +1%
	B_1	00-10 1:3	+20%	Carbon Dust 1:100
	B_2	00-10 1:1	+0%	PMS488C +1%
	C	00-10 1:1	+10%	None
7-9	A	00-30 1:1	+10%	PMS488C +1%
	B_1	00-10 1:3	+20%	Carbon Dust 1:100
	B_2	00-30 1:1	+0%	PMS488C +1%
	C	00-30 1:1	+10%	None

B. Test Method, Reference Tools, and Controls

Performance of the TIS in image mosaicking and background elasticity measurement are tested separately on each of the 9 phantom samples. For mosaicking accuracy, total path length and 2D positioning errors are considered, with estimations from the TIS algorithm compared with positioning data from a VICON 3D photogrammetry system with typically 0.5mm accuracy [36]. Here path length is total scalar distance travelled, and position error is the residual position error magnitude at the end of a scan. The scan consisted of 25 passes, with approximately 50% overlap between passes to cover the sample area. This was the target overlap, however with the manual application of the TIS, deviations between 40% and 60% were typical. Scans deviating beyond this were rejected. This error adds to the 'realism' and therefore represents performance in real use. 5 scans were made of each sample, maintaining consistent loading 10±2N and tilt angles (θ, φ) 0±5°, with scan rates approximately 0.03m/s. Water based lubricant was used to minimize the effect of shear on the TIS and material. The TIS was recalibrated according to Section VI-A before each scan.

For elasticity measurement, 5 repeat comparisons are made between the TIS estimate and the response from an Instron 3342 universal testing machine (Instron Engineering Corp., UK), with typical 0.5% accuracy. This was fitted with an identical indenter tip to the TIS and compared at equivalent strains, applied to the center of the samples. The TIS was pressed slowly, normally, into each sample, with no lateral motion up to a load of 15N with tilt angle maintained 0±2° at a nominal rate of 5mm/s. Water based lubricant is used to stop the surface sticking. The TIS was recalibrated before each repeated measurement. The test material was relaxed between tests.

For all tests and reference measurements, for elasticity or position, temperature was maintained at 22°C to maintain the tactile sensor calibration, and phantom mechanical properties.

VIII. Results

A. Image Registration Accuracy

The results of 5 repeated scans of the 9 samples in terms of total path length error compared with the VICON reference is shown in Fig.7. A first order surface trend shows that the path reconstruction improves as the base material becomes firmer, as a result of lower general distortion to the surface at a given load, however the trend is relatively small. Variation in feature density has negligible effect on path length estimation.

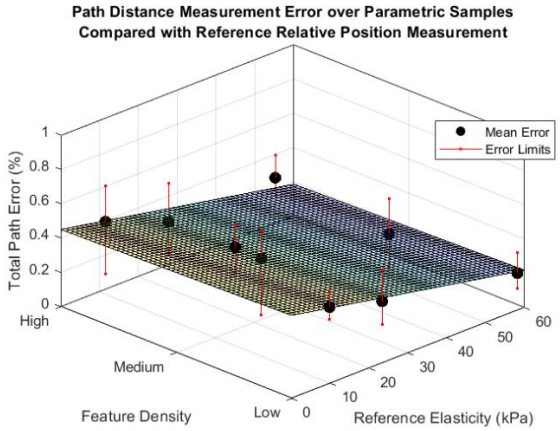

Fig. 7 - Total path length error vs. background elasticity and representative feature density. Path length estimation generally improves as base material becomes firmer.

Analysis of the repeated scans from the view point of positioning error is shown in Fig.8, where the RMS error is a measure of the difference in end location in 2D space between the TIS estimation and the VICON reference of the TIS position. The results show that the error reduces slightly as the base material elasticity increases, although the effect is small. This is again due to lower general distortion and shearing on stiffer materials at a fixed scan load. Increasing feature density generally improves position error, although the effect is small over the range of materials tested.

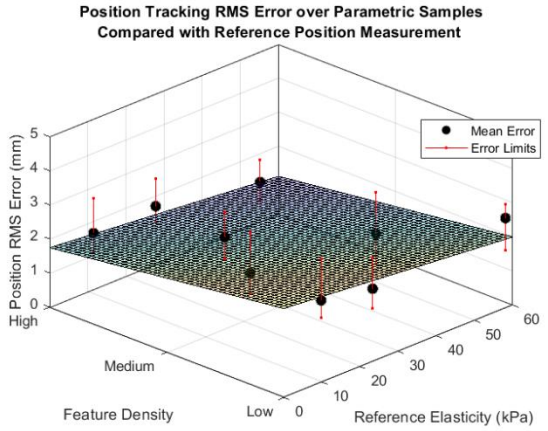

Fig. 8 - Position RMS tracking error vs background elasticity and representative feature density. Positioning accuracy generally improves with feature density and base material firmness.

Continuing the analysis, the average response of the TIS and proposed algorithms over all sample materials is compared against performance without the deformation reduction algorithm from Section IV-A, using SIFT only. Similar comparisons are made against the performance of previous design iterations [21] over their respective test materials. This is shown in Table 2.

RMS error provides a metric for relative image position accuracy on the surface, whilst error ratio (or total path error) is a metric for evaluating the linear segment registration error. These were chosen as registration evaluation metrics, rather than direct image comparison methods with a static vein image, as they are not affected by lighting or camera projection differences and can be generalized for use on 3D reconstruction applications where simple reference images are not available.

Table 2 - Comparison of TIS with previous system and methods

COMPARISON OF POSITIONING ERROR TO PREVIOUS METHODS AND PROTOTYPES			
System / Metric	**TIS with Proposed Algorithm**	**TIS with SIFT**	**Existing Large Prototype [20]**
ERROR RATIO (%)	0.337	1.686	0.296
RMS ERROR (mm)	2.091	10.467	2.261

The results show that the TIS and proposed algorithm is effective in comparison to the TIS hardware using SIFT alone, showing that the deformation reduction algorithm is effective. It also shows that the path error (error ratio) increases with the reduction in image capture area between the previous work [21] and the TIS, and increase in surface deformation for a fixed load between the TIS and previous work [21]. The scan area is reduced by a factor of 9.45, but the total path error ratio only increases by a factor of 1.14 which is a good result, indicating that there is sufficient features on the phantoms for the algorithm to track. Interestingly, the RMS error is improved slightly using the TIS and algorithm compared with previous works. This is attributed to reduced friction for the TIS reducing the shear deformation.

B. Background Elasticity Accuracy

The results of the comparison between repeat uses of the TIS and Instron reference in terms of elasticity measurement are shown in Fig.9. The results show that the absolute error increases slightly as the reference material increases, with negligible deviation across the feature densities tested in this work. This is attributed to the reduction in measurable strain over a fixed load range as materials become stiffer, meaning the measurement noise in tracking image features has a slightly larger relative effect than for softer materials with larger deformations. Minimal deviation with variation in feature density is attributed to each sample having sufficient features to track the macroscopic average deformation. The TIS has a propensity to read elasticity slightly high, as shown in Fig.9, compared with individual reference measurements from the Instron; attributable to the choice of $\nu = 0.5$. Minor deviations in this nominal value (0.48-0.5) for elastic silicone depending on mixture consistency easily explains this deviation.

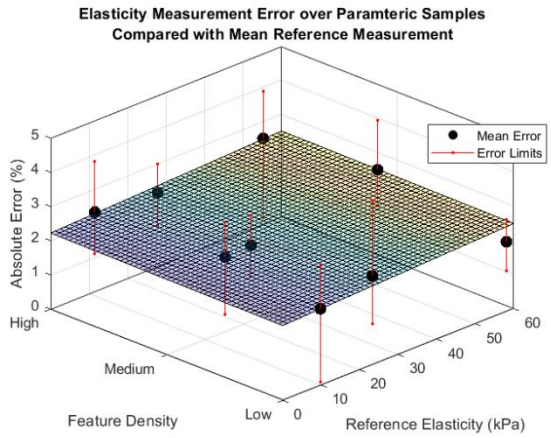

Fig. 9 – TIS elasticity measurement accuracy vs. reference and feature density.

General results of the reference elasticity measurements, and subsequent stability of the TIS measurement are shown in Table 3. These results provide the reference elasticity in previous analyses, and show that there is increasing variability in elasticity estimates from the TIS as elasticity increases, attributable to increased vibration as the base material stiffens.

Table 3 – TIS Elasticity Measurement vs. Reference Elasticity

ELASTICITY MEASUREMENT RESULTS FOR PROPOSED SYSTEM ON PARAMETRIC SAMPLES COMPARED WITH REFERENCE MEASUREMENTS						
SAMPLE FEATURE DENSITY PARAMETER	**SAMPLE ELASTICITY PARAMETER**					
	SOFT		**MEDIUM**		**HARD**	
	Measured (kPa)	**Reference (kPa)**	**Measured (kPa)**	**Reference (kPa)**	**Measured (kPa)**	**Reference (kPa)**
LOW	**10.0** +0.12 -0.21	**9.8** +0.2 -0.1	**22.7** +0.33 -0.51	**23.3** +0.2 -0.2	**56.9** +0.49 -0.38	**58.1** +0.1 -0.4
MEDIUM	**15.5** +0.15 -0.26	**15.2** +0.1 -0.1	**22.4** +0.19 -0.20	**21.9** +0.1 -0.2	**56.4** +0.79 -0.58	**54.8** +0.2 -0.1
HIGH	**11.2** +0.14 -0.17	**11.5** +0.2 -0.1	**27.2** +0.27 -0.23	**27.8** +0.3 -0.1	**56.6** +0.76 -1.27	**55.2** +0.2 -0.3

IX. Discussion

A. Results Discussion

The results from section VI-B have shown that the TIS and proposed algorithms are capable of mosaicking composite tactile images and referencing them onto the background vein network, validated in silicone phantoms. As the tactile array is not used for the process, the registration is robust to variation in contact load particularly when compared to existing registration methods [10]. The validity and accuracy of the tactile mosaic is independent of the tactile array and this was validated on representative silicone samples parametrically to determine sensitivity to breast background stiffness and vein density. The registration accuracy generally improves as the elasticity of the test material increases, and also as the average vein density increases. The lower material deformation, and subsequently smaller amount of deformation reduction required from stiffer materials at a fixed load seems to allow the TIS to perform slightly better at higher base elasticities. Similarly, materials with higher feature densities have more features to track between frames improving the certainty of any transform.

The elasticity measurement accuracy decreased slightly with increasing material stiffness. This could be attributed to two sources, firstly the increased vibration of the TIS on stiffer materials (from lower damping) or, secondly from the value of Poisson ratio changing slightly with different mixture ratios. The variability in elasticity from the TIS compared with the reference is likely dictated by the former, and the static 'high' reading is governed by the latter.

The results presented still represent a significant step forward in tactile imaging, by allowing for robust tactile image registration and estimation of background elasticity to reasonable accuracy that can be used in further clinical analysis of breast TI, without significant increase in component costs.

B. Experimental Limitations

The phantom materials themselves were the main experimental limitation in this work. It was necessary to begin analysis on a simple case of a flat plane, with linear properties, to reduce the number of problem variables. The TIS is expected to generalize to forming 3D surface images, and has the necessary hardware to do so. Similarly, the TIS is expected to be capable of characterizing non-linear materials due to the continuous measurement of stress and strain during the elasticity measurement process, although further work is required to verify this assertion. Another limitation was that an optimal tactile array was not available, and so meaningful analysis of the tactile mosaic, in terms of inclusion characterization, could not be done. This did not affect the outcome of generating the tactile mosaic, and so is a minor limitation. The final limitation is the range of phantom materials tested. Parametric analysis is resource intensive, and so only a limited number of calibrated samples could be produced which is sufficient to tell if there is sensitivity in the TIS response, but not enough to fully characterize it.

C. Outcomes and Significance

This work has presented a viable method for mosaicking tactile images, and performed parametric analysis on the sensitivity of the TIS response to variable conditions. This has allowed for a solid base of understanding with which to further develop breast TI. The fact that the proposed method is not reliant on visible tactile features makes this method more robust than previous methods that were sensitive to operator process [10], without losing significant performance from the compaction of early prototypes [21], further validating that initial process. This work now allows TI to view the whole breast, and provides the required base measurement for lesion elasticity [10] required for greater diagnostic accuracy and monitoring of conditions over time [1].

X. Conclusion and Future Work

This work has addressed two major limitations in current breast TI, in forming composite images of the full breast (in phantom trials) and estimating background elasticity which allows for a full breast view and future estimation of lesion elasticity respectively [10]. Further developments will allow data to be combined at the scan probe, making synchronization automatic and allowing the system to operate in real time. The further development of TI requires the following validations: The current TIS should be tested on 3D breast phantoms to form truly representative breast maps, where more complex material phantoms can be produced with inclusions [13]; The TIS should implement a suitable high resolution tactile array, with subsequent analysis of inclusions/lesions to verify that the TIS composite image is effective compared to a single static image for estimation of lesion properties using traditional TI methods [10]; and then the TIS should be clinically validated on patients to demonstrate the expected improvement in diagnostic/differential accuracy versus existing TI methods [1], [12] and other methods such as ultrasound. This will verify the effectiveness of the delivered metrics generally. Beyond this, the TIS has applications during treatment as well as in detection as the vein image mosaic can be used to measure hemodynamic response, for monitoring treatment using chemotherapy [23].

References

[1] V. Egorov *et al.*, 'Differentiation of benign and malignant breast lesions by mechanical imaging', *Breast Cancer Res. Treat.*, vol. 118, no. 1, pp. 67–80, Nov. 2009, doi: 10.1007/s10549-009-0369-2.

[2] J. S. Brandt, T. Rosen, H. V. Raalte, V. Kurtenos, and V. Egorov, 'Characterization of Perineum Elasticity and Pubic Bone-Perineal Critical Distance with a Novel Tactile Probe: Results of an Intraobserver Reproducibility Study', *Open J. Obstet. Gynecol.*, vol. 10, no. 04, pp. 493–503, 2020, doi: 10.4236/ojog.2020.1040044.

[3] V. Egorov, S. Ayrapetyan, and A. P. Sarvazyan, 'Prostate mechanical imaging: 3-D image composition and feature calculations', *IEEE Trans. Med. Imaging*, vol. 25, no. 10, pp. 1329–1340, Oct. 2006, doi: 10.1109/TMI.2006.880667.

[4] R. Hampson, R. G. Anderson, and G. Dobie, 'Non-Invasive Radial Artery Blood Pressure Monitoring Using Error Compensated Tactile Sensors and Patient Specific Oscillometry', in *2022 44th Annual International Conference of the IEEE Engineering in Medicine & Biology Society (EMBC)*, Glasgow, Scotland, United Kingdom, Jul. 2022, pp. 828–831. doi: 10.1109/EMBC48229.2022.9871598.

[5] H. Yang, Y. Xu, Y. Zhao, J. Yin, Z. Chen, and P. Huang, 'The role of tissue elasticity in the differential diagnosis of benign and malignant breast lesions using shear wave elastography', *BMC Cancer*, vol. 20, no. 1, p. 930, Dec. 2020, doi: 10.1186/s12885-020-07423-x.

[6] M. Guray and A. A. Sahin, 'Benign breast diseases: classification, diagnosis, and management', *The oncologist*, vol. 11, no. 5, pp. 435–449, 2006.

[7] A. Sahu *et al.*, 'Characterization of Mammary Tumors Using Noninvasive Tactile and Hyperspectral Sensors', *IEEE Sens. J.*, vol. 14, no. 10, pp. 3337–3344, Oct. 2014, doi: 10.1109/JSEN.2014.2323215.

[8] R. W. Sanderson *et al.*, 'Camera-based optical palpation', *Sci. Rep.*, vol. 10, no. 1, p. 15951, Dec. 2020, doi: 10.1038/s41598-020-72603-5.

[9] C.-H. Won, J.-H. Lee, and F. Saleheen, 'Tactile Sensing Systems for Tumor Characterization: A Review', *IEEE Sens. J.*, vol. 21, no. 11, pp. 12578–12588, Jun. 2021, doi: 10.1109/JSEN.2021.3078369.

[10] V. Egorov and A. P. Sarvazyan, 'Mechanical Imaging of the Breast', *IEEE Trans. Med. Imaging*, vol. 27, no. 9, pp. 1275–1287, Sep. 2008, doi: 10.1109/TMI.2008.922192.

[11] B. Verma, P. McLeod, and A. Klevansky, 'Classification of benign and malignant patterns in digital mammograms for the diagnosis of breast cancer', *Expert Syst. Appl.*, vol. 37, no. 4, pp. 3344–3351, Apr. 2010, doi: 10.1016/j.eswa.2009.10.016.

[12] M.-K. Tasoulis, K. E. Zacharioudakis, N. G. Dimopoulos, and D. J. Hadjiminas, 'Diagnostic accuracy of tactile imaging in selecting patients with palpable breast abnormalities: a prospective comparative study', *Breast Cancer Res. Treat.*, vol. 147, no. 3, pp. 589–598, Oct. 2014, doi: 10.1007/s10549-014-3123-3.

[13] M. K. Sharma *et al.*, 'Experimental Investigation of the Breast Phantom for Tumor Detection Using Ultra-Wide Band–MIMO Antenna Sensor (UMAS) Probe', *IEEE Sens. J.*, vol. 20, no. 12, pp. 6745–6752, Jun. 2020, doi: 10.1109/JSEN.2020.2977147.

[14] A. Sarvazyan and V. Egorov, 'Mechanical imaging-a technology for 3-D visualization and characterization of soft tissue abnormalities: a review', *Curr. Med. Imaging Rev.*, vol. 8, no. 1, pp. 64–73, 2012.

[15] C. R. Gentle, 'Mammobarography: a possible method of mass breast screening', *J. Biomed. Eng.*, vol. 10, no. 2, pp. 124–126, Apr. 1988, doi: 10.1016/0141-5425(88)90086-6.

[16] V. Lefemine, G. Osborn, A. Mainwaring, and S. Goyal, 'Have Standardised Referral Forms Reduced the Number of Inappropriate Referrals to Breast Clinic?', *Bull. R. Coll. Surg. Engl.*, vol. 94, no. 2, pp. 1–3, Feb. 2012, doi: 10.1308/147363512X13189526438954.

[17] A. Sarvazyan, V. Egorov, J. S. Son, and C. S. Kaufman, 'Cost-effective screening for breast cancer worldwide: current state and future directions', *Breast Cancer Basic Clin. Res.*, vol. 1, p. 91, 2008.

[18] A. M. Franz, T. Haidegger, W. Birkfellner, K. Cleary, T. M. Peters, and L. Maier-Hein, 'Electromagnetic Tracking in Medicine—A Review of Technology, Validation, and Applications', *IEEE Trans. Med. Imaging*, vol. 33, no. 8, pp. 1702–1725, Aug. 2014, doi: 10.1109/TMI.2014.2321777.

[19] O. Mandrik *et al.*, 'Systematic reviews as a "lens of evidence": Determinants of cost-effectiveness of breast cancer screening', *Cancer Med.*, vol. 8, no. 18, pp. 7846–7858, Dec. 2019, doi: 10.1002/cam4.2498.

[20] V. Egorov, H. van Raalte, and A. P. Sarvazyan, 'Vaginal Tactile Imaging', *IEEE Trans. Biomed. Eng.*, vol. 57, no. 7, pp. 1736–1744, Jul. 2010, doi: 10.1109/TBME.2010.2045757.

[21] S. Rana, R. Hampson, and G. Dobie, 'Breast Cancer: Model Reconstruction and Image Registration From Segmented Deformed Image Using Visual and Force Based Analysis', *IEEE Trans. Med. Imaging*, vol. 39, no. 5, pp. 1295–1305, May 2020, doi: 10.1109/TMI.2019.2946629.

[22] V. P. Zharov, S. Ferguson, J. F. Eidt, P. C. Howard, L. M. Fink, and M. Waner, 'Infrared imaging of subcutaneous veins', *Lasers Surg. Med.*, vol. 34, no. 1, pp. 56–61, Jan. 2004, doi: 10.1002/lsm.10248.

[23] F. Teng *et al.*, 'Wearable near-infrared optical probe for continuous monitoring during breast cancer neoadjuvant chemotherapy infusions', *J. Biomed. Opt.*, vol. 22, p. 9, 2017.

[24] A. Agudo, F. Moreno-Noguer, B. Calvo, and J. M. M. Montiel, 'Sequential Non-Rigid Structure from Motion Using Physical Priors', *IEEE Trans. Pattern Anal. Mach. Intell.*, vol. 38, no. 5, pp. 979–994, May 2016, doi: 10.1109/TPAMI.2015.2469293.

[25] N. Haouchine, J. Dequidt, M.-O. Berger, and S. Cotin, 'Single view augmentation of 3D elastic objects', in *2014 IEEE International Symposium on Mixed and Augmented Reality (ISMAR)*, Munich, Germany, Sep. 2014, pp. 229–236. doi: 10.1109/ISMAR.2014.6948432.

[26] N. Micheletti, J. H. Chandler, and S. N. Lane, 'Structure from Motion (SfM) Photogrammetry', *Geomorphol. Tech.*, p. 13, 2015.

[27] G. Yu and J.-M. Morel, 'ASIFT: An Algorithm for Fully Affine Invariant Comparison', *Image Process. Line*, vol. 1, Feb. 2011, doi: 10.5201/ipol.2011.my-asift.

[28] B. Triggs, P. F. McLauchlan, R. I. Hartley, and A. W. Fitzgibbon, 'Bundle Adjustment — A Modern Synthesis', in *Vision Algorithms: Theory and Practice*, vol. 1883, B. Triggs, A. Zisserman, and R. Szeliski, Eds. Berlin, Heidelberg: Springer Berlin Heidelberg, 2000, pp. 298–372. doi: 10.1007/3-540-44480-7_21.

[29] H. Xiao, G. Ren, and J. Cai, 'A review on 3D deformable image registration and its application in dose warping', *Radiat. Med. Prot.*, vol. 1, no. 4, pp. 171–178, Dec. 2020, doi: 10.1016/j.radmp.2020.11.002.

[30] E. Karami, S. Prasad, and M. Shehata, 'Image Matching Using SIFT, SURF, BRIEF and ORB: Performance Comparison for Distorted Images', p. 5, 2017.

[31] OnSemi, '1/2.5-Inch 5 Mp CMOS Digital Image Sensor MT9P031', 2019. https://www.onsemi.com/pdf/datasheet/mt9p031-d.pdf (accessed Jan. 12, 2023).

[32] A. Llagostera Casanovas and A. Cavallaro, 'Audio-visual events for multi-camera synchronization', *Multimed. Tools Appl.*, vol. 74, no. 4, pp. 1317–1340, Feb. 2015, doi: 10.1007/s11042-014-1872-y.

[33] M.A.Fischler and R.C. Bolles, 'Random Sample Consensus: A Paradigm for Model Fitting with Applications to Image Analysis and Automated Cartography', *Comm ACM*, vol. 24, pp. 381–395, 1981.

[34] B. Ustbas, D. Kilic, A. Bozkurt, M. E. Aribal, and O. Akbulut, 'Silicone-based composite materials simulate breast tissue to be used as ultrasonography training phantoms', *Ultrasonics*, vol. 88, pp. 9–15, Aug. 2018, doi: 10.1016/j.ultras.2018.03.001.

[35] R. Hampson, G. Dobie, and G. West, 'Elasticity Measurement of Soft Tissues Using Hybrid Tactile and MARG-Based Displacement Sensor Systems', *IEEE Sens. J.*, vol. 19, no. 22, pp. 10262–10270, Nov. 2019, doi: 10.1109/JSEN.2019.2930207.

[36] R. Summan *et al.*, 'Spatial calibration of large volume photogrammetry based metrology systems', *Measurement*, vol. 68, p. 12, 2015.

AUTHOR BIOGRAPHIES

Rory Hampson received the PhD and MEng degrees from the University of Strathclyde, Glasgow, U.K., in 2021 and 2017 respectively. He is currently a researcher in the Department of Electronic and Electrical Engineering at the University of Strathclyde. His current work focusses on tactile imaging for breast cancer diagnosis, medical decision making based on tactile sensor technology, and automated inspection robots. His research interests are Medical Imaging, Inertial Guidance and Control, Nuclear Inspection, and Engineering Sustainable Development.

Graeme West received the B.Eng. (Hons.) and Ph.D. degrees from the University of Strathclyde, Glasgow, U.K., in 1998 and 2002, respectively. He is a Senior Lecturer in the Department of Electronic and Electrical Engineering at the University of Strathclyde. His research interests include intelligent system applications in condition monitoring, diagnostics and prognostics.

Gordon Dobie received the Ph.D. degree in electrical and mechanical engineering from the University of Strathclyde with a focus on development of reconfigurable non-contact inspection system. He is currently a Reader with the department of Electronic and Electrical Engineering, University of Strathclyde. He is currently with CUE, where he is involved in automated ultrasonic inspection of complex geometries. His primary research interests are ultrasonics, NDE, automation, robotics, signal processing, computer vision and embedded systems.